Supervised Learning Project (AE 419)

CFD Analysis of Flows Through Bell Nozzle with Cooling

project by

V S Harikrishna - 160010054

Instructor : Prof. V. R. Kowsik Bodi

Department of Aerospace Engineering
Indian Institute of Technology, Bombay

May 2023

Contents

List of Figures

List of Tables

List of Symbols

δ	The boundary layer thickness at a given streamwise location x
δ^*	The displacement thickness of the boundary layer at a given streamwise location x
μ	The dynamic viscosity of the fluid
ν	The kinematic viscosity of the fluid
ρ	The local density of the fluid at a given streamwise location x
τ_{wall}	The wall shear stress exerted by the fluid on the surface of the flat plate
θ	The momentum thickness of the boundary layer at a given streamwise location x
$c_{f,\theta}$	The the coefficient of friction between fluid and plate surface computed using the slope of the momentum thickness vs streamwise location x
$c_{f,\tau}$	The the coefficient of friction between fluid and plate surface computed using wall shear stress exerted by the fluid on the surface of the flat plate
H	The shape factor of the boundary layer at a given streamwise location x
$R_e(x)$	The Reynolds' Number of the flow at the given streamwise location x
U_∞	The free stream velocity above the plate at a given streamwise location x
u_y	The streamwise flow velocity at a given vertical location y above the plate for constant streamwise location x
x	Streamwise coordinate, taken positive along the flow
y	Vertical coordinate, taken positive upwards
z	Span-wise coordinate, positive direction as per right hand coordinate system

Abstract

The present study focuses on the numerical simulation of nozzle flow using ANSYS Fluent, a state-of-the-art computational fluid dynamics (CFD) software. The primary objective of this project is to analyze and understand the complex fluid dynamics and performance characteristics of a converging-diverging nozzle under various operating conditions. Nozzle flows are of critical importance in engineering applications, including aerospace propulsion systems, fuel injectors, and industrial processes.

The research methodology involves the creation of a three-dimensional geometric model of the nozzle, incorporating the converging and diverging sections, inlet, and outlet. The governing equations of fluid flow, the Navier-Stokes equations, are discretized using finite volume methods and solved numerically to predict the fluid's behavior within the nozzle.

The project investigates several key parameters influencing nozzle performance, including inlet pressure, outlet pressure, mass flow rate, and geometry variations. Through a series of simulations, the project evaluates the effects of these parameters on flow characteristics such as velocity profiles, pressure distribution, Mach number distribution, and mass flow rate through the nozzle.

The results obtained from ANSYS Fluent simulations are validated against analytical solutions and experimental data from the literature, demonstrating the accuracy and reliability of the numerical approach. Sensitivity analyses are conducted to identify critical design and operational parameters affecting nozzle performance and efficiency.

This project contributes to a comprehensive understanding of nozzle flow behavior and its significance in engineering applications. The knowledge gained from this study can aid in the optimization of nozzle designs, leading to improved performance and efficiency in various industrial processes and propulsion systems. Furthermore, the utilization of ANSYS Fluent as a powerful CFD tool for nozzle flow analysis showcases its potential for simulating complex fluid dynamics in a wide range of engineering and scientific domains.

1 INTRODUCTION

1.1 Rao Nozzle

Propelling nozzle have formed the base of Rocket and Jet propulsion for decades. Propelling nozzle is a nozzle which converts thermal and pressure energy of the flow into kinetic energy of the flow. Power available in the gas turbine exhaust is converted into a high speed propelling jet by the nozzle. Propelling nozzles can be subsonic, sonic, or supersonic. Physically the nozzles can be convergent, or convergent-divergent(C-D). C-D nozzles can give supersonic jet velocity within the divergent section, whereas in a convergent nozzle the exhaust fluid cannot exceed the speed of sound within the nozzle. Propelling nozzles can be fixed geometry, or they can have variable geometry to give different throat areas most typically to control the effects of large temperature rises in the jet pipe with afterburner or reheat operation. Nozzles for supersonic flight speeds,at which high nozzle pressure ratios are generated, also have variable area divergent sections.

A typical nozzle operates by using its throat to increase pressure within the engine by constricting airflow, usually until the flow chokes, then expanding the exhaust stream to, or near to, atmospheric pressure, while forming it into a high speed jet to propel the vehicle. The energy to accelerate the stream comes from the temperature and pressure of the gas. The gas expands adiabatically with low losses and hence high efficiency. The gas accelerates to a final exit velocity which depends on the pressure and temperature at entry to the nozzle, the ambient pressure it exhausts to, and the efficiency of the expansion.

For a typical rocket nozzle high exit velocities as required the overall velocity requirement for the rocket is high. This is due to the nature of mission that the rocked has, either to carry a ballistic payload to a part on earth within few minutes or to place a satellite in orbit. Due to this high exit velocity requirement the rocked nozzle needs to have a very high area ratio diverging section for it to achieve such velocities. Most of the modern rockets travel at hypersonic speeds.

This problem was existent during the cord war period and many people were involved in making a superior rockets and which shed light into areas on more efficient nozzle for rockets. In 1955s on such person, Dr.G.V.R. Rao, made the mathematical foundation to the modern day rocket nozzles while working at Rocketdyne.

The Bell-shaped or Contour nozzle is probably the most commonly used shaped rocket engine nozzle. It has a high angle expansion section (20 to 50 degrees) right behind the nozzle throat; this is followed by a gradual reversal of nozzle contour slope so that the nozzle exit the divergence angle is small, usually less than a 10 degree half angle.

Ideally a nozzle is wished to direct all of the gases generated in the combustion chamber and accelerated by the throat to leave the nozzle traveling straight out the nozzle. That means the momentum of the gases are axial, imparting the maximum thrust to the rocket. In fact, there are some non-axial components to the momentum. In terms of a momentum vector, there is an angle between the axis of the rocket engine and the flow of the gas. As a result, the thrust is lowered by varying amounts. The Bell or Contour shape is designed to impart a large angle expansion for the gases right after the throat. The nozzle is then curved back in to give a nearly straight flow of gas out the nozzle opening. The contour used is rather complex. The large expansion section near the throat causes expansion shock waves. The reversal of the slope to bring the exit to near zero degrees causes compression shock waves.

A properly designed nozzle will have these two sets of shock waves coincide and cancel each other out. In this way, the bell is a compromise between the two extremes of the conical nozzle since it minimizes weight while maximizing performance. The most important design issue is to contour the nozzle to avoid oblique shocks and maximize performance.

Theoretically the Bell/Rao nozzle should be able to achieve it but when analysed using a CFD analysis will it still be more efficient? The efficiency of a bell nozzle needs to be compare with a conical nozzle of the same area ratio and length in order to qualitatively understand the importance of these nozzles.

Although similar studies might be carried out earlier this study is an honest approach in getting to know the concepts of propulsion in a new light and to compare the real world results to the idealistic solutions obtained in classroom studies. Therefore the motivation of the current work is to learn more real world insights and to study the effectiveness of the above mentioned Bell/Rao Nozzle.

1.2 Numerical simulation of Flow through Nozzle

Governing Equations

For an Isentropic flow:

$$\frac{p_2}{p_1} = \left(\frac{\rho_2}{\rho_1}\right)^{\gamma} = \left(\frac{T_2}{T_1}\right)^{\frac{\gamma}{\gamma-1}} \tag{1}$$

Total conditions in a flow are related to static conditions via:

$$\begin{aligned} \frac{T_0}{T} &= 1 + \frac{\gamma-1}{2}M^2 \\ \frac{p_0}{p} &= \left(1 + \frac{\gamma-1}{2}M^2\right)^{\frac{\gamma}{\gamma-1}} \\ \frac{\rho_0}{\rho} &= \left(1 + \frac{\gamma-1}{2}M^2\right)^{\frac{1}{\gamma-1}} \end{aligned} \tag{2}$$

For steady adiabatic flow, energy equation can be written as:

$$h_0 = h + \frac{V^2}{2} \tag{3}$$

For a calorically perfect gas total temperature is constant across a normal shock wave while there is a loss in total pressure. Basic Normal Shock equations are:

$$\begin{aligned} M_2^2 &= \frac{1+\frac{\gamma-1}{2}M_1^2}{\gamma M_1 - \frac{\gamma-1}{2}} \\ \frac{p_2}{p_1} &= 1 + \frac{2\gamma}{\gamma+1}(M_1^2 - 1) \end{aligned} \tag{4}$$

Quasi One Dimensional Flow: If area variation is moderate, the components other than axial direction are often neglected. This assumption give rise to Quasi 1D flow where all flow field variables vary primarily along one direction. we have taken this assumption to obtain the analytical results. The isentropic flow of a calorically perfect gas through a CD nozzle is governed by following equation:

$$\frac{A}{A^*} = \frac{1}{M}\left[\frac{2}{\gamma+1} + \frac{\gamma-1}{\gamma+1}M^2\right]^{\frac{\gamma+1}{2(\gamma-1)}} \tag{5}$$

This relation is called as area Mach number relation. It tells us that Mach no. inside a duct is governed by the ratio of local duct area(A) to the sonic throat area (A^*). The closed form expression for mass flow through a choked nozzle is given

by:

$$\dot{m} = \frac{p_0 A^*}{\sqrt{T_0}} \sqrt{\frac{\gamma}{R}\left(\frac{2}{\gamma+1}\right)^{\frac{\gamma+1}{\gamma-1}}} \tag{6}$$

Clearly mass flow rate depends on the Total Pressure, Temperature, Sonic Throat area and Gas properties.

1.3 Boundary Layer Thickness

The effect of a boundary layer can be characterised by its thickness. The thickness of the boundary layer over a flat plate is defined by different means. The boundary layer thickness, the displacement thickness and momentum thickness and the energy thickness. These definitions assume that the flow is incompressible and use velocity profile, continuity equation, momentum equation and energy equation respectively to define the effect of the boundary layer.

– **Boundary Layer Thickness:** The distance measured perpendicular to the surface at which the velocity of the flow achieves 99 percent of the free stream velocity is defined as the boundary layer thickness (δ). The boundary layer thickness can be visualised properly in Fig 1.

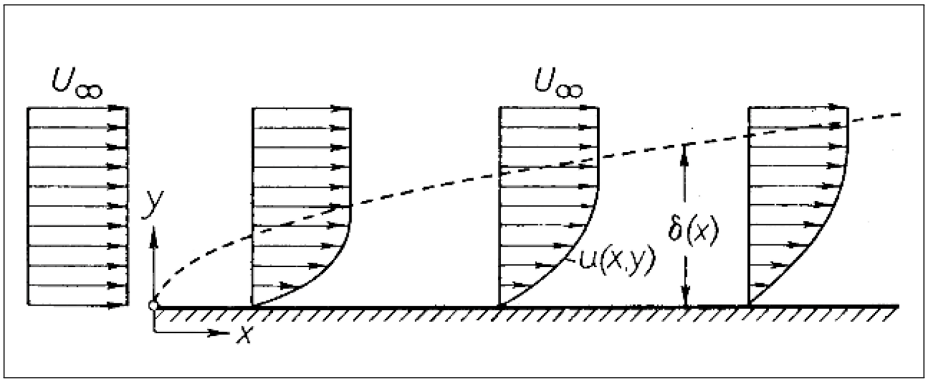

Figure 1: Boundary layer thickness [2]

– **Displacement Thickness:** The displacement thickness (δ^*) is the amount of divergence the flow undergoes in order to satisfy continuity equation. It is the additional separation undergone by streamlines originally supposed to be present where the boundary layer exists to maintain the same mass flow rate between

them in presence of the shear induced velocity gradient. This is made clear by Fig 2

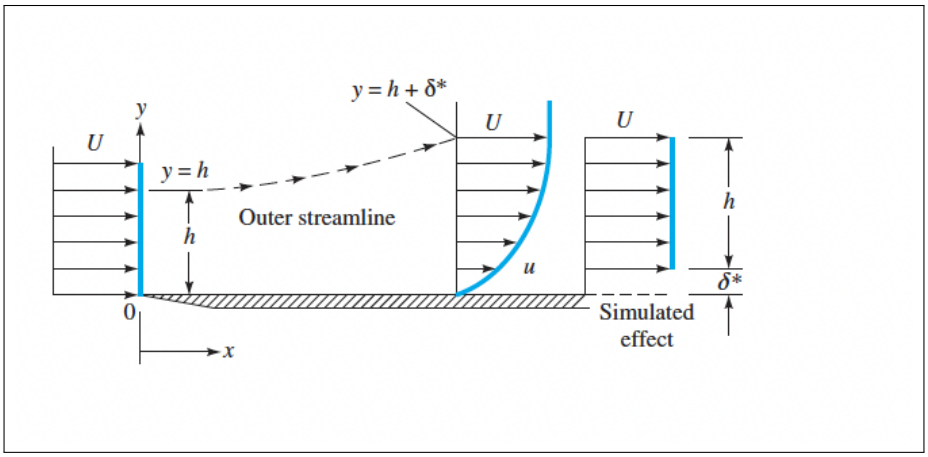

Figure 2: Displacement thickness [6]

– **Momentum Thickness:** The shear effects of the flow cause the fluid to lose momentum to the wall. This results in a reduction of fluid velocity and forms a velocity gradient. The momentum thickness (θ) is the effective thickness of the undisturbed flow measured perpendicular to the wall that simulates this momentum deficit from the flow. This is made clear by Fig 3

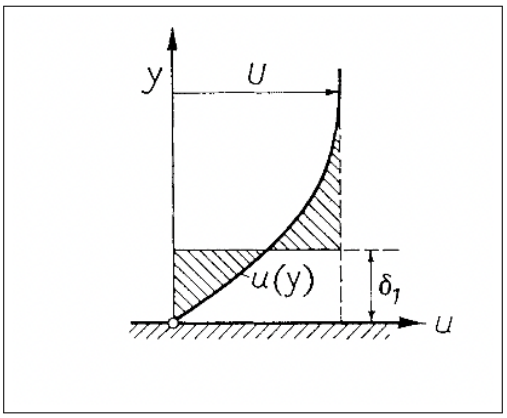

Figure 3: Momentum thickness [4]

– **Energy Thickness:** Like momentum, the shear effects of the flow cause the fluid to lose energy to the wall. This results in a reduction of fluid velocity and forms a velocity gradient. The momentum thickness (δ^{**}) is the effective thickness of the undisturbed flow measured perpendicular to the wall that simulates this energy deficit from the flow.

1.4 Shape Factor

The ratio of displacement thickness to momentum thickness is defined as the shape factor (H) of the boundary layer. The shape factor characterises the transition from laminar to turbulent flow within the boundary layer. The shape factor values of 1.4-1.3 is typical for turbulent flows and that of 2.4-1.5 is typical for laminar flows. The Blasius' laminar solution has a shape factor of 2.59.

1.5 Wall Shear Stress and Coefficient of Friction

The wall shear stress (τ_{wall}) is defined as per Eqn **??**. The viscous nature of the fluid results in a shear stress governed by fluid viscosity and velocity gradient normal to the wall surface. This is defined as the wall shear stress shown by Fig 16. The shear effects results due to the force applied by the flow tangential to the wall surface. This force can be thought of as the wall frictional force. The force when normalised with the dynamic head, id defined as the coefficient of wall friction given by Eqns 17 and 18

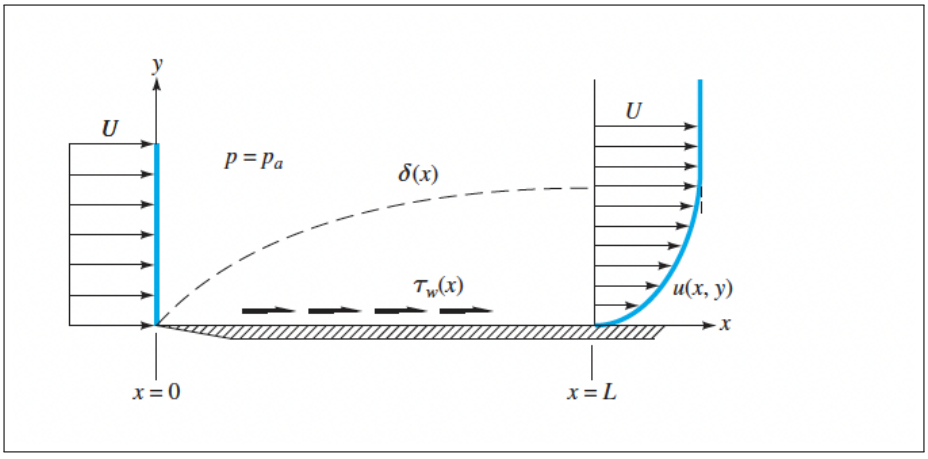

Figure 4: Wall shear stress[6]

1.6 Experimental Calculations

The calculation of ambient density from the ambient temperature is done using the Ideal Gas Equation of State[5].

$$\rho = \frac{p}{RT} \tag{7}$$

The calculation of flow velocity from the measured dynamic pressure is done using the given equation[5]:

$$\Delta p = \frac{\rho * u^2}{2} \tag{8}$$

$$\text{where } \Delta p = p_0 - p_{amb}$$

The dynamic viscosity for flow μ is given using the Sutherland's formula[3]:

$$\mu = \mu_0 \left(\frac{T_0 + C}{T + C}\right)\left(\frac{T}{T_0}\right)^{\frac{3}{2}} \tag{9}$$

where $\mu_0 = 1.716 \times 10^{-5} kg/ms$, $T_0 = 273.15K$ and $C = 110.4$

The kinematic viscosity for flow ν is given using the following formula:

$$\nu = \frac{\mu}{\rho} \tag{10}$$

The Reynolds' Number for flow R_e is given using the following formula [5]:

$$R_e = \frac{\rho u_{\infty x}}{\mu} \tag{11}$$

The boundary layer thickness at a given streamwise coordinate (x) is given using the following formula from theory [6]:

$$\delta = \frac{\rho u_{\infty x}}{\mu} \tag{12}$$

The displacement thickness at a given streamwise coordinate (x) is given using the following formula from theory [6]:

$$\delta^* = \int_0^{\delta} (1 - \frac{u(y)}{U_\infty}) dy \tag{13}$$

The momentum thickness at a given streamwise coordinate (x) is given using the following formula from theory [6]:

$$\theta = \int_0^{\delta} (\frac{u(y)}{U_\infty})(1 - \frac{u(y)}{U_\infty}) dy \tag{14}$$

The shape factor (H) of at a given streamwise coordinate (x) is given using the following formula from theory [6]:

$$H = \frac{\delta^*}{\theta} \tag{15}$$

The wall shear stress (τ_{wall}) of at a given streamwise coordinate (x) is given using the following formula from theory [3]:

$$\tau_{wall} = \mu \left(\frac{\delta u}{\delta y} \right)_{wall} \tag{16}$$

The local coefficient of friction (c_f) of at a given streamwise coordinate (x) is given using the following two formulae from theory [3]:

$$c_{f,\tau} = 2\frac{\tau_{wall}}{\rho U_\infty^2} \tag{17}$$

$$c_{f,\theta} = 2\frac{d\theta}{dx} \tag{18}$$

The velocities and lengths are non-dimensionalised as the following

$$\text{Non-dimensionalised velocity} = \frac{u}{U_\infty} \tag{19}$$

$$\text{Non-dimensionalised y-coordinate}(\eta) = \frac{y\sqrt{R_e}}{x} \tag{20}$$

$$\text{Non-dimensionalised x-coordinate} = \frac{x}{x_{max}} \tag{21}$$

$$\text{Non-dimensionalised displacement thickness} = \frac{\delta^*}{\delta} \tag{22}$$

$$\text{Non-dimensionalised momentum thickness} = \frac{\theta}{\delta} \tag{23}$$

The integrals involved in above formulae are evaluated using the trapezoidal rule for integration, and the backward difference to compute derivatives as shown in the expressions below.

$$\int f(x)dx = \sum \frac{x_{i+1} - x_i}{2}[f(x_{i+1}) + f(x_i)] \tag{24}$$

$$\frac{df(x_i)}{dx} = \frac{f(x_i) - f(x_{i-1})}{x_i - x_{i-1}} \tag{25}$$

1.6.1 Theoretical Predictions

For laminar flow, the boundary layer thickness is given as per theory [6]:

$$\delta_{Th,lam} = \frac{5x}{\sqrt{R_e}} \tag{26}$$

For laminar flow, the displacement thickness normalised with respect to boundary layer thickness is given as per theory [4]:

$$\left(\frac{\delta^*}{\delta}\right)_{Thory,lam} = 0.351 \tag{27}$$

For laminar flow, momentum thickness normalised with respect to boundary layer thickness is given as per theory [6]:

$$\left(\frac{\theta}{\delta}\right)_{Th,lam} = 0.133 \tag{28}$$

For laminar flow, shape factor is given as per theory [6]:

$$H = 2.6 \tag{29}$$

For laminar flow, coefficient of friction is given as per theory [6]:

$$c_f = \frac{1.721}{\sqrt{R_e}} \tag{30}$$

For turbulent flow, the boundary layer thickness is given as per theory [6]:

$$\delta_{Th,turb} = \frac{0.16x}{R_e^{\frac{1}{7}}} \tag{31}$$

For turbulent flow, the displacement thickness normalised with respect to boundary layer thickness is given as per theory [4]:

$$\left(\frac{\delta^*}{\delta}\right)_{Th,turb} = 0.125 \tag{32}$$

For turbulent flow, momentum thickness normalised with respect to boundary layer thickness is given as per theory [6]:

$$\left(\frac{\theta}{\delta}\right)_{Th,turb} = \frac{7}{72} \tag{33}$$

For turbulent flow, shape factor is given as per theory [6]:

$$H = 2.6 \tag{34}$$

For turbulent flow, coefficient of friction is given as per theory [6]:

$$c_f = \frac{0.027}{R_e^{\frac{1}{7}}} \tag{35}$$

1.7 Experiment Setup

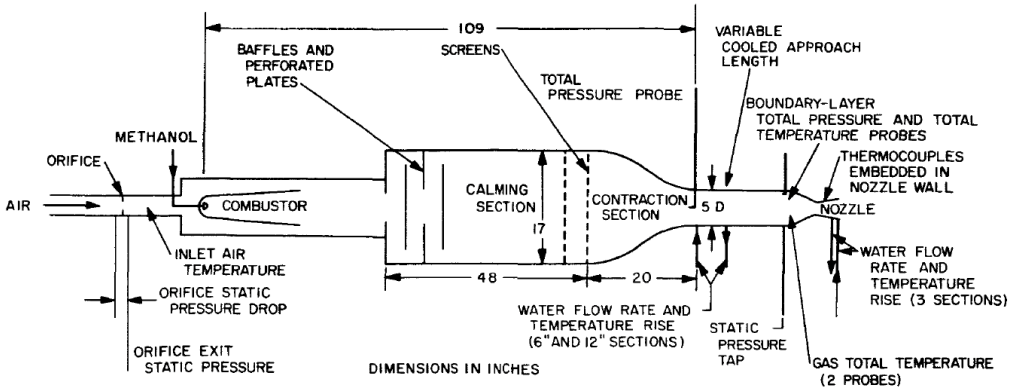

Fig. 1. Flow and instrumentation diagram

Figure 5: Flat plate and coordinate system setup

1.8 Experimental Setup

In this investigation, which covered a range of stagnation pressures from 30 to 250 psia and stagnation temperatures from 1030 to 2000°R, compressed air was heated by the internal combustion of methanol and then mixed to obtain uniformity before it entered the nozzle. The mixing and distance of the combustion from the nozzle minimized maldistributions, and the ratio of methanol-to-air weight flow rate was small enough, even for the highest stagnation temperature, so that the products of combustion could be treated approximately as air. The nozzle had a throat diameter of 1.803 in., a contraction-area ratio of 7.75 to 1, an expansion-area ratio of 2.68 to 1, a convergent half-angle of 30 deg, and a divergent half-angle of 15 deg. The exit Mach number was about 2.5. Local convective heat-transfer results were obtained by measuring steady-state temperatures with thermocouples embedded in plugs pressed into the water-cooled nozzle wall. Radiation effects were negligible over the stagnation-temperature range. To determine the effect of boundary-layer thickness at the nozzle inlet on heat transfer in the nozzle, the length of the constant-diameter cooled approach section upstream of the nozzle inlet was changed in 6-in. lengths from 0 to 18 in.

1.9 Geometry specifications and Meshing

Parameter	Values used
Length of Nozzle	$0.150495m$
Inlet and Outlet Radius	$0.064m$ and $0.037296m$
Throat Radius and Location	$0.0229m$ and $0.09075m$
Convergent and Divergent Half angle	30° and 15°
Expansion and Contraction area Ratio	2.68 and 7.75
Radius of curvature along inlet	$0.036068m$
Radius of curvature along throat	$0.04572m$

Meshing

Parameter	Values used
Radial elements	50
Axial elements	$104(12+35+25+32)$

2 FLUENT SIMULATION

2.1 Getting Familiar: FLUENT tutorials

CFD was something that I was learning form scratch so in order to facilitate faster learning Prof. Bodi suggest me to go through FLUENT tutorials. The set of tutorials that he had suggested me was a part of 'SimCafe' of Cornell University. These set of tutorials that I had tried were from the series "Computational Fluid Mechanics using FLUENT"

It had many different different Tutorials each dealing with different type of basics problems which gave insight on the FLUENT and CFD basics. The tutorials that was suggested and which were completed were:

1. Laminar Pipe Flow
2. Flat Plate Boundary Layer
3. Supersonic Flow over a Wedge
4. Compressible Flow in a Nozzle

2.2 Flow Simulation in Bell/Rao Nozzle

2.2.1 Introduction

Bell Nozzles are parabolic shaped converging diverging nozzles mostly used in rocket engines. They are considered to be one of the most efficient nozzles. This Nozzle's mathematics was created mostly by G.V.R. Rao, hence is also called as Rao nozzles.

2.2.2 Defining the geometry

Using ANSYS workbench create a project file for the above problem statement and save a copy. The dimensions of the Nozzle are:

Length = 0.150495m

Inlet and Outlet Radius = 0.064m and 0.037296m

Throat Radius and Location = 0.0229m and 0.09075m

Convergent and Divergent Half angle = 30°and 15°

Expansion and Contraction area Ratio= 2.68 and 7.75

Radius of curvature along inlet = 0.036068m

Radius of curvature along throat = 0.04572m The nozzle data was obtained from an M.tech student Mr.Deepak Yadav who is also working under Prof. Bodi. The Geomertry that was thus created looks something like in fig

2.2.3 Creating a Mesh for the Nozzle

Once the design of the geometry is done then the mesh modelling can be done. The default mesh generated by ANSYS is not refined, hence we generate a mapped face meshing for it. Also, the sizing of the mesh is then defined according to the grid size that is required. The number of divisions that we had chosen were 50 along radial direction and 104 along axial direction.

Then named selection are created for the edges, Pressure inlet, Pressure outlet, Axis and Nozzle Wall as shown in the figure below.

2.2.4 Physics Setup.

The physics setup of the nozzle is done step by step. Once FLUENT is open, we see in general pane there is an option for selecting the type of solver that is to be used. As the flow we deal in nozzles are compressible flows we select Density based solver. We have also considered the 2D space as Axi-symmetric, hence that is also selected in the solver. The time steeping here is steady, all these are set up in the solver section in FLUENT as shown in fig 5.4.1a.

Next the types of model that are used are defined, we only use energy model in our case hence that is selected(fig 5.4.1b), although viscous fluid may be considered.

Properties of the fluid is defined now and the gaseous properties is set to be defined by ideal gas law (fig 5.4.1c). Then we define the boundary conditions for each of the named selections that we had selected. The named selections have defined the type of boundary that we will be using. But initially 'pressure far field' condition ran into errors and the solution didn't converge, after some research, some trial and error, and upon Bodi Sir's idea the pressure far field boundary condition was changed to pressure outlet and was input in the Boundary conditions.

But later upon further research in CFD online forums[1] and ANSYS FLUENT User guide[2] we were able to figure out the error was due to improper initialisation as the FLUENT solver in standard initialization will not consider subsonic to supersonic or supersonic to subsonic transitions unless the inlet and exit values show that there exist a transition. Using a Hybrid initialisation these errors were solved completely. And the results obtained by both are compared at the end of this chapter.

2.2.5 Boundary Conditions

The boundary conditions that were defined at inlet and exit for the first case were as follows:

Boundary	Parameter	Values used
Inlet	p_0	$518485.7Pa$
Inlet	T_0	$842K$
Outlet	p	$101325Pa$,
Outlet	T_0	$300K$
Wall	Temperature (constant)	$394K$
Wall	Heat Generated (constant)	$-30W/m^3$
Wall	Thickness (constant)	$0.0074168m$

2.3 Computing Numerical Solution.

Once the physics values and boundary conditions are set up, we then move to the final phase in computing the flow. Getting the numerical solution.

2.3.1 Solution Methods and Monitors.

The solution method that is used is and implicit solver and the flux type is Roe-FDS. The spatial discretization schemes that were used were second order upwind and third order MUSCL, and the gradient type being least square cell based.

Only one type of monitor was defined and they were 'Residuals-print, plot'. During computation these monitors print and plotted the error residual for all computing values. The absolute requirement for convergence was changed from 0.001 to 1e-6.

2.3.2 Initialisation

There are two types of solution initialisation that are available in ANSYS FLUENT for density based solvers, standard and hybrid. Standard initialisation sets same initial value at all points and hybrid computes the probable value at some points along the flow and sets initial value accordingly.

Standard initialisation has its limitation when there is a transition form subsonic to supersonic hence hybrid initialisation is used.

After initialising the values we move on to run calculation pane. Here we set the number of initialization to 1000. A point to note is that there exits an option called solution steering which is available only for density based steady problems. Selecting this option and selecting the type of flow from the option will actually help in convergence of the solution quicker

Once calculate option is clicked the software starts computing and the residuals are plotted as shown in fig 5.5.1f. After few number of iterations depending upon the grid size, the initialisation and weather solution steering is used or not the solution will converge.

2.4 1D flow Analysis

For a 1D flow analysis, T0and P0are constant throught the length of the nozzle, only static values vary. And the static pressure varies (for given back pressure varies as)

Now the velocity at the inlet is assumed to be M0 = 0.455, hence using isentropic flow relations we find that at the throat flow is chocked and M_{th} = 1.0, now looking for $\frac{A}{A^*}$ = 25 in isentropic flow tables we get exit mach number as M_e = 5.0.

2.5 Solutions obtained

Below are the plots and graphical contours that are obtained for different conditions for a Bell nozzle

2.5.1 Initial case: Using Non-Conductive Walls

Contours:

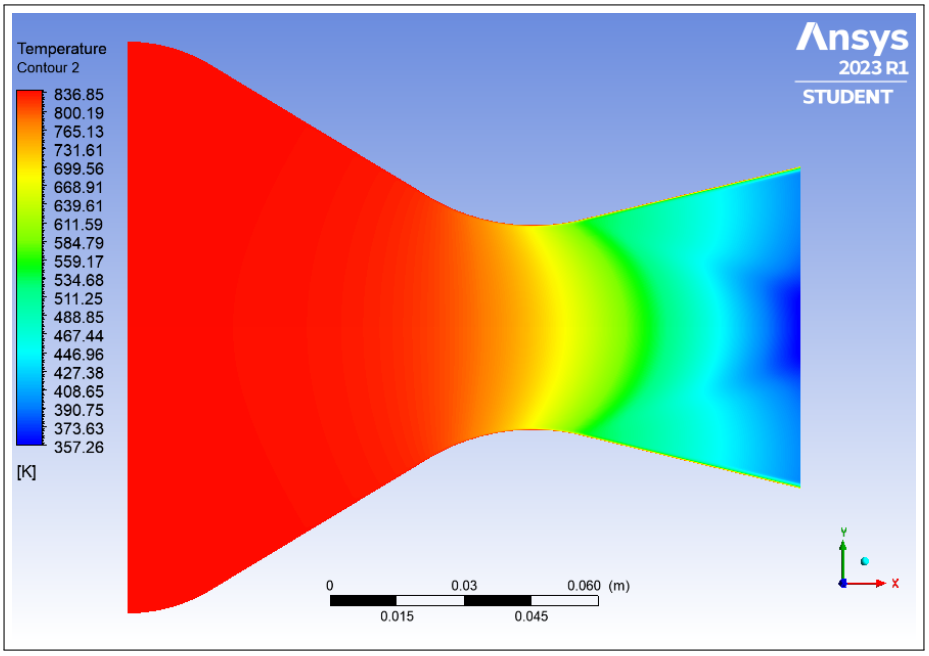

Figure 6: Temperature contours

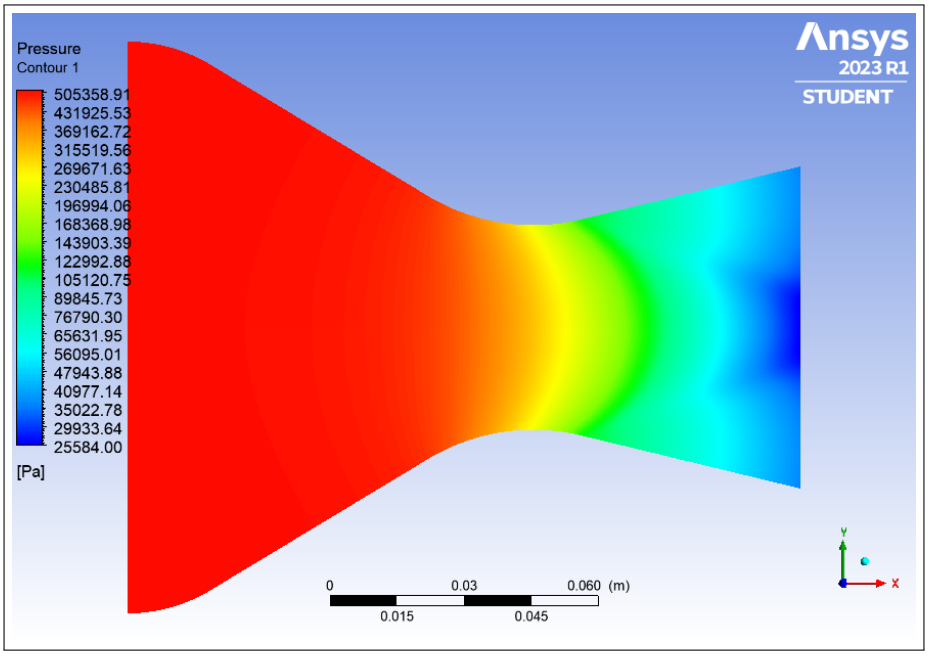

Figure 7: Pressure contours

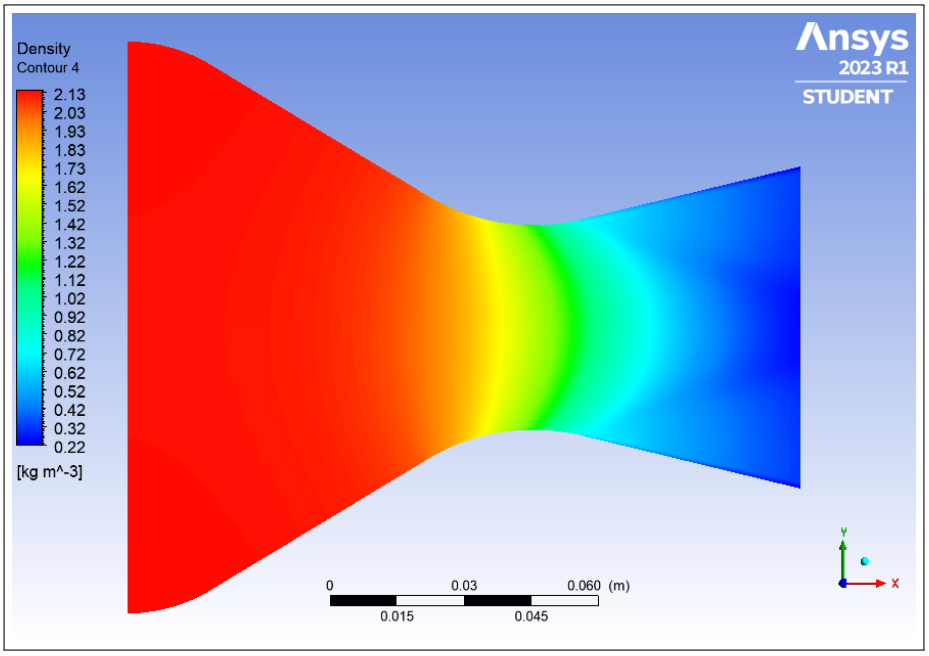

Figure 8: Density contours

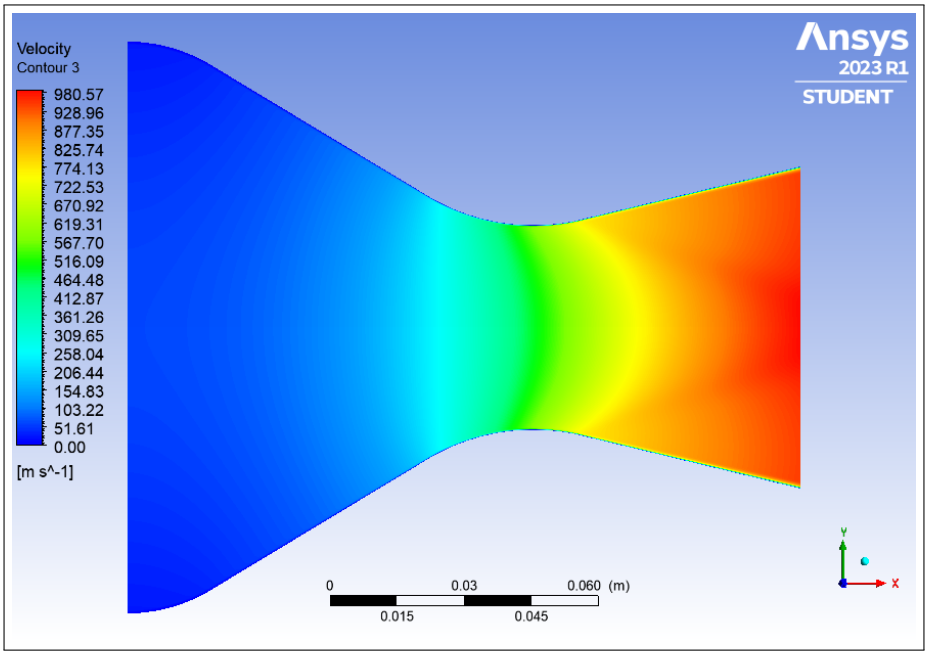

Figure 9: Velocity contours

2.5.2 Second case: Using Conductive Walls with Cooling

Once it was known that the pressure outlet can be used as pressure outlet in boundary condition and convergence can still be achieved. The error was not in the boundary condition but was in initialisation.So another simulation was carried out for Bell nozzle using hybrid initialisation. The plots and figures obtained were as follows. A comparison is done subsequently to the older case

Contours:

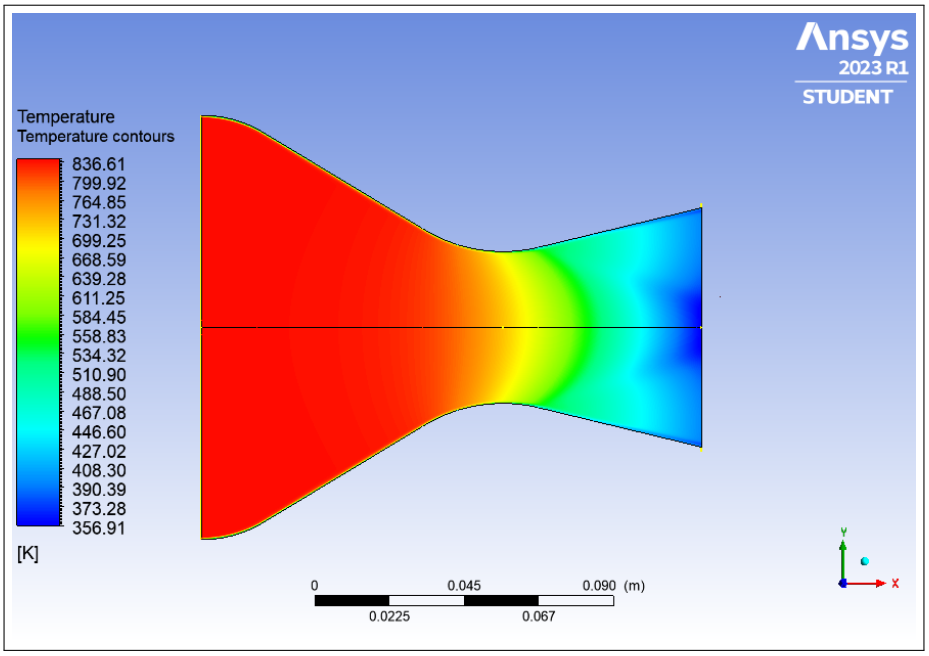

Figure 10: Temperature contours

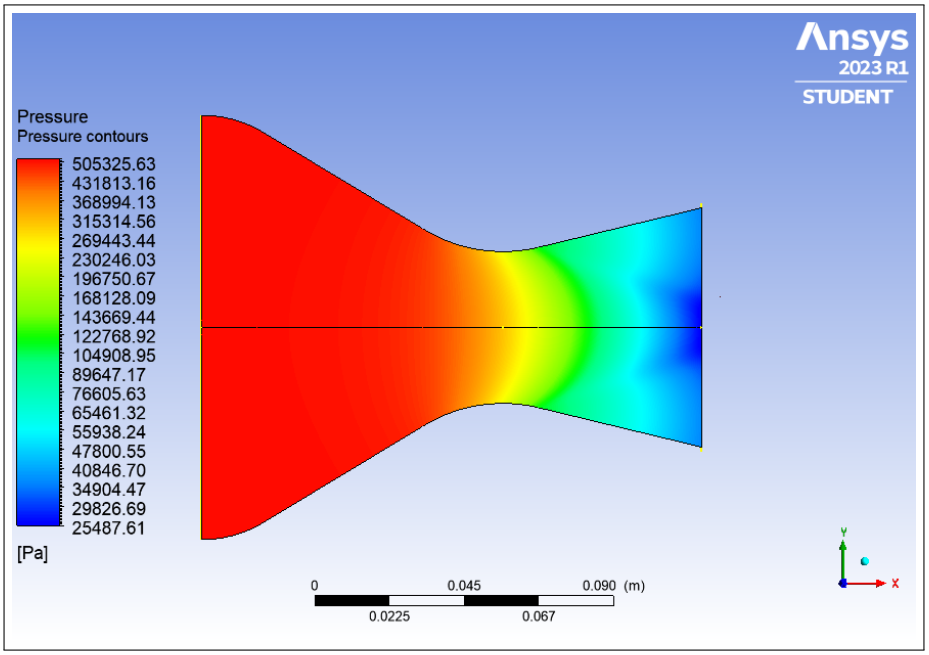

Figure 11: Pressure contours

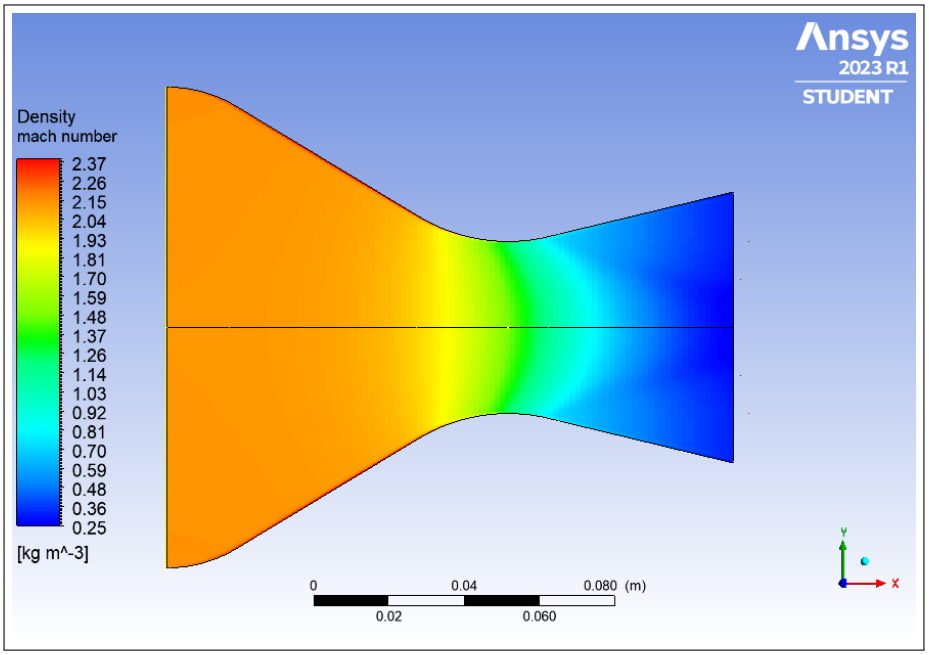

Figure 12: Density contours

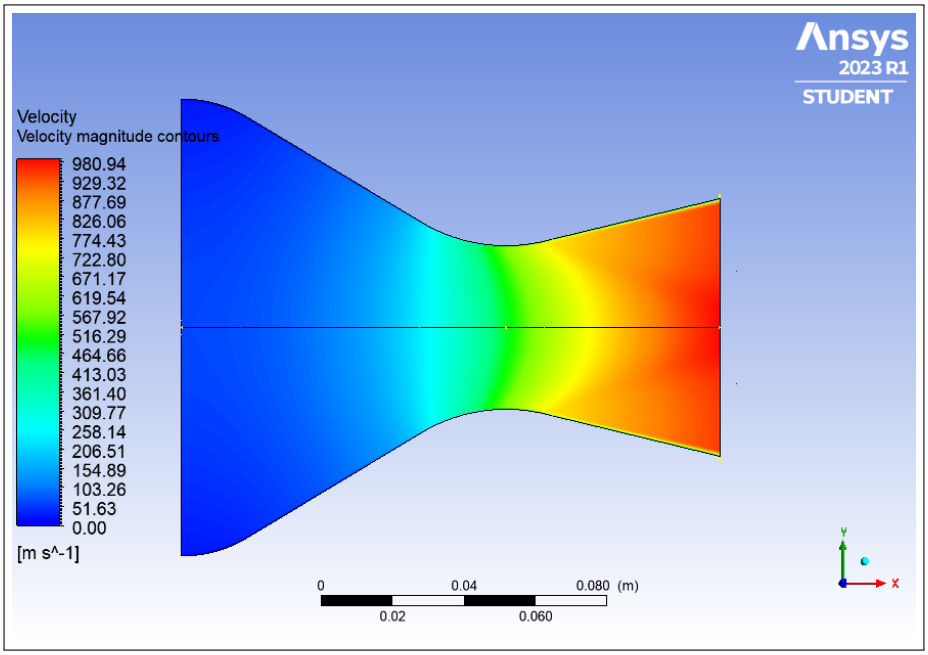

Figure 13: Velocity contours

3 RESULTS AND COMPARISONS

3.1 Plots

3.1.1 Pressure Ratio vs x-coordinate

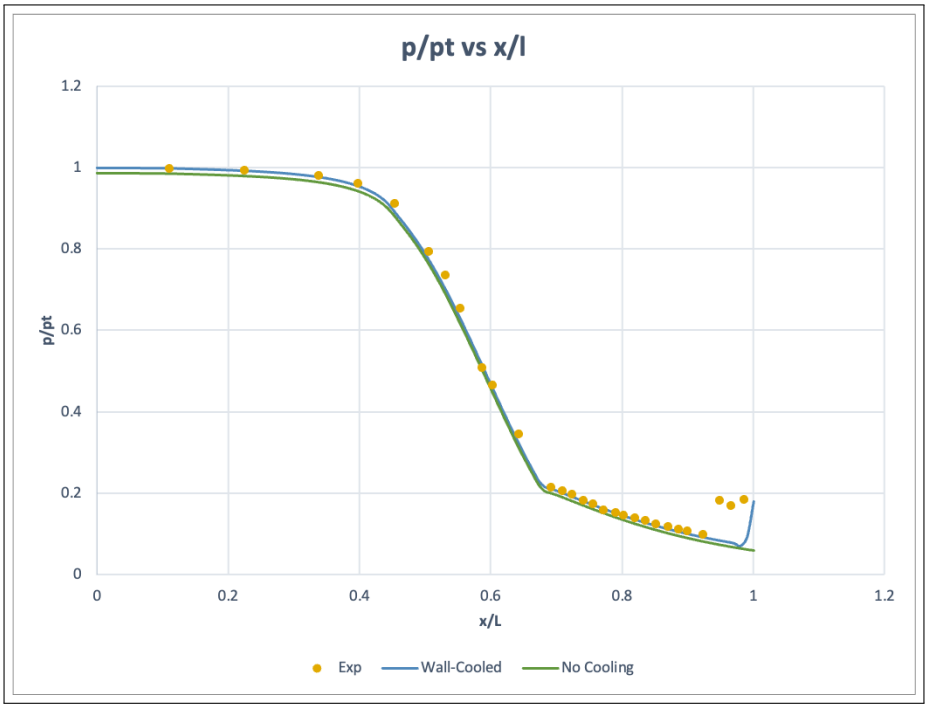

Figure 14: Normalised y coordinate (η) vs normalised velocity $\frac{u}{U_\infty}$ plots for different values of x compared with Blasius (1908) Profile [1] for (a) Expt 1, (b)Expt 2

The velocity distribution is observed to coincide roughly showing a self similar nature. Although, deviations are observed for the case of $x = 3.4cm$ due to the effect of leading edge flow reversal observed during the experiment. The profile seems to agree with the Blasius [1] profile as expected by the theory when away from the plate and vary from it when close to the plate. This might be due to the inability of the Pitot probe to reach very close to the plate due to its finite thickness. These velocity profiles are normalised with respect to the similarity parameters η and U_∞.

3.1.2 Normalised Plots of wall shear vs x

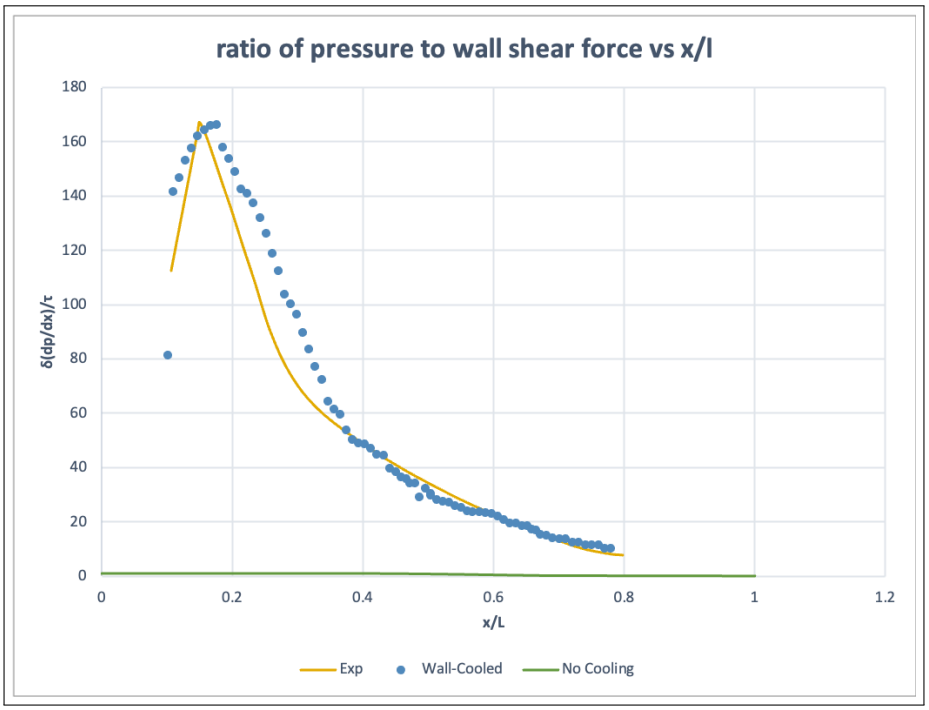

Figure 15: Normalised momentum thickness $\frac{\theta}{\delta}$ vs normalised x coordinate $\frac{x}{x_{max}}$ plots for different values of x compared with theoretical plots for laminar and turbulent[6] flow for (a) Expt 1, (b)Expt 2

The momentum thickness is normalised with respect to the boundary layer thickness as per Eqn 23 and x is normalised with respect to x_{max}. The experimental plot is observed to approach the turbulent theoretical plot for increasing values of x. This is due to the fact that Reynolds' number increases with x and flow becomes more turbulent. Although, deviations are observed for very large values of x and this is thought to be due to mixing of flow with ambient air. The plot does not seem to start from the laminar values as expected by the theory. This might be due to the inability of the Pitot probe to reach very close to the plate due to its finite thickness. Another reason might be due to the observed reverse flow conditions near the leading edge of the plot as mentioned previously and discussed in section 7.

3.1.3 Heat transfer coefficient (h) vs x

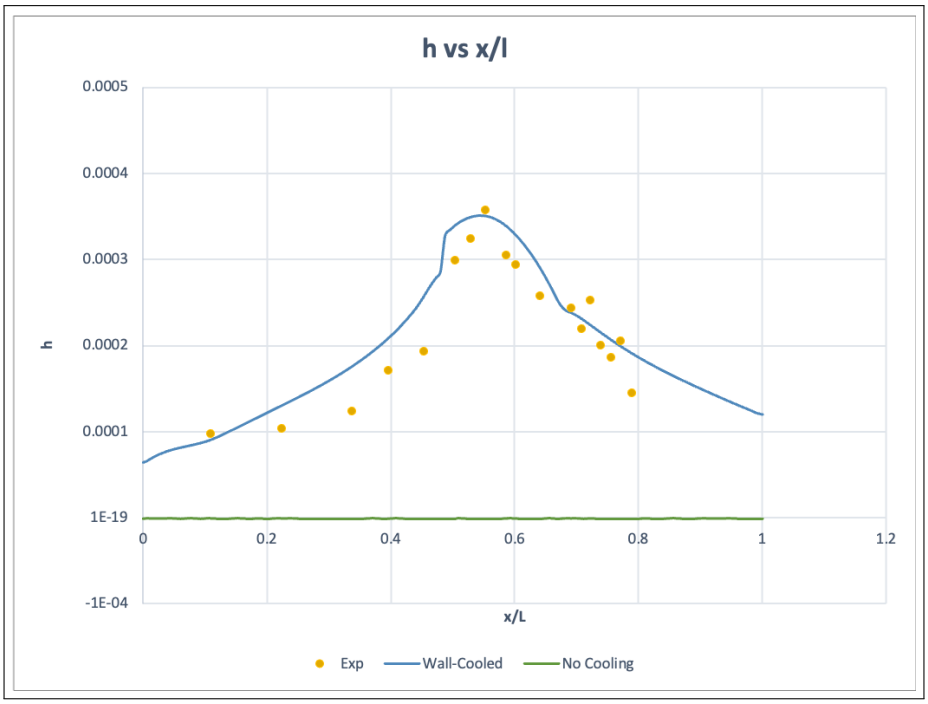

The shape factor is observed to be close to the turbulent theoretical plot and appears to approach the turbulent plot for increasing values of x. This is due to the fact that Reynolds' number increases with x and flow becomes more turbulent. Although, deviations are observed for very large values of x and this is thought to be due to mixing of flow with ambient air. The plot does not seem to start from the laminar values as expected by the theory. This might be due to the inability of the Pitot probe to reach very close to the plate due to its finite thickness. Another reason might be due to the observed reverse flow conditions near the leading edge of the plot as mentioned previously and discussed in section 7.

3.2 Grid Independence Study

In order to prove grid independence, the number of axial and radial divisions were parametrized in FLUENT and the pressure distribution over the wall surface was studied to observe settling. It was observed that at about 100 axial divisions and 50 radial divisions, further refinement of the grid yielded no significant change in the output parameters. A plot is given to show the same.

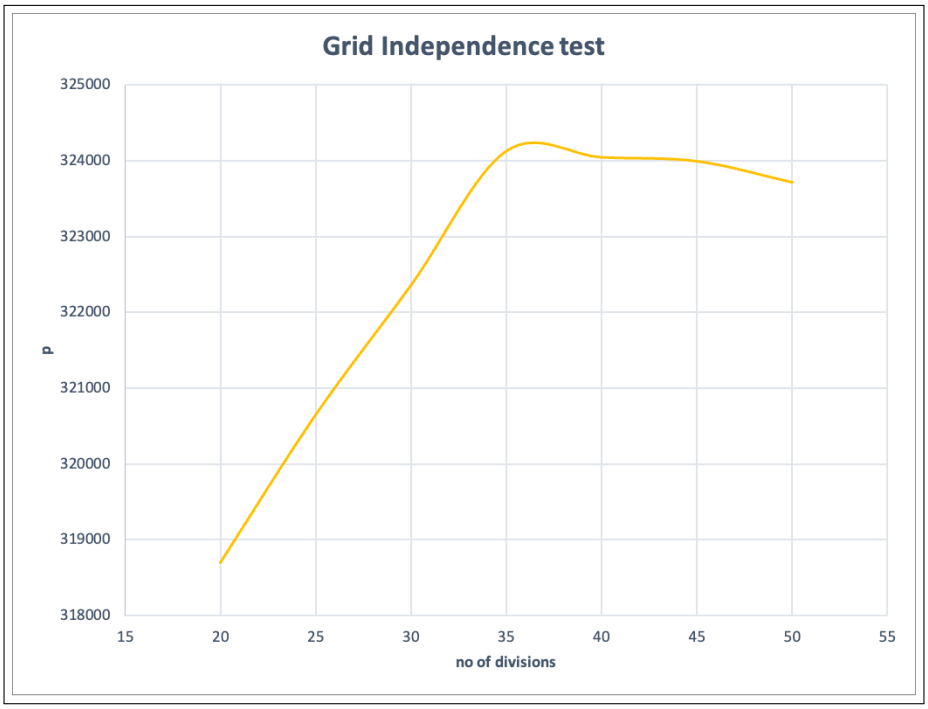

Figure 16: Wall shear stress[6]

4 CONCLUSIONS & DISCUSSION

4.1 Comparison between plots

From the experimental plots and simulation plots the following can be inferred:

1. Once we compare these values obtained from computation to a 1D flow analysis we find a few things which are different.
2. The exit Mach number Me, is supposed to be equal to 2.6, which is computed by using the area ratios of throat to nozzle exit, but from 1D Nozzle analysis the average value of mach number at exit plane is 2.52.
3. The variation of Mach number normal to the axis is observed because of the variation on of static temperature as exit velocity of almost all particle at exit is nearly the same
4. The Nozzle total pressure ratio is ideally equal to 1, but here there is a slight drop in nozzle total pressure. The drop in nozzle total pressure ratio indicates the the flow may not be perfectly isentropic as assumed. This is shown in the image:

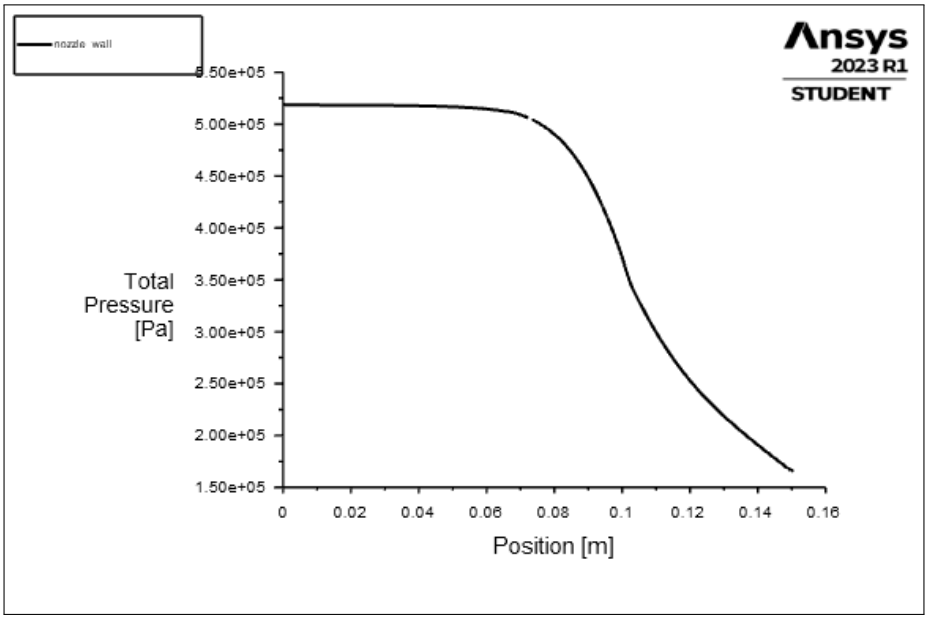

Figure 17: Total pressure at the wall

5. Although, the total pressure away from wall appears to be conserved. Thereby showing isentropic flow behaviour. This is shown in the image:

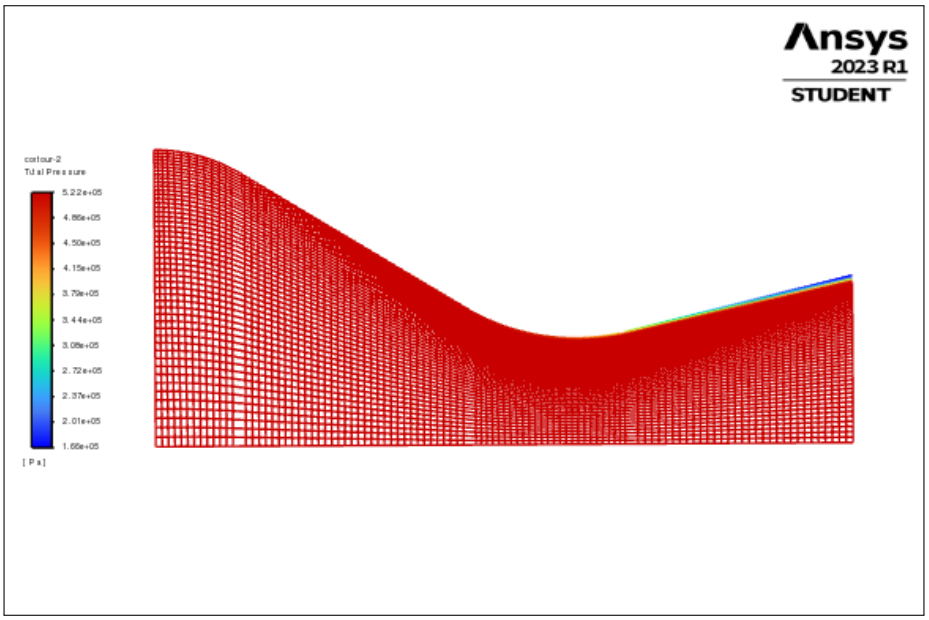

Figure 18: Total pressure at the wall

6. However, velocity increases along x as expected.
7. The total temperature decreases along the wall due to wall conduction in case of the wall cooled case. However, even in case of the non-conducting wall, case, there was a slight decrease in total temperature due to viscous irreversibilities.

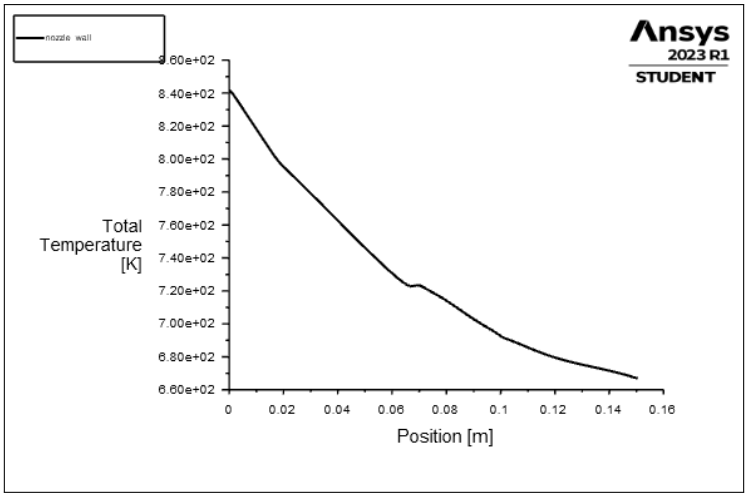

Figure 19: Total temperature at the wall

8. When compare to the earlier pressure far-field conditions the only changes that we might notice is slight variation in the static temperature behaviour, the pressure behaviour wont change as the entry and exit pressure conditions are the same.

References

[1] H. Blasius. The boundary layers in fluids with little friction. *Zeitschrift für Mathematik und Physik*, 56, 1908.

[2] Hermann Schlichting (Deceased) and Klaus Gersten. *Boundary-Layer Theory*. Springer-Verlag GmbH Berlin Heidelberg, ninth edition, 2017.

[3] ANSYS Inc. Ansys fluent user's guide. Canonsburg, Pennsylvania, U.S., 2009.

[4] Ronald L. Panton. *Incompressible Flow*. John Wiley Sons, Inc, fourth edition, 2013.

[5] Prof. Prabhu Ramachandran. Lecture slides of ae 225 (incompressible fluid mechanics). Department of Aerospace Engineering, 2020.

[6] Frank M. White. *Fluid Mechanics*. McGraw-Hill, Inc., eighth edition, 2011.